Science Advances
AAAS

advances.sciencemag.org/cgi/content/full/6/11/eaaz0087/DC1

Supplementary Materials for

Temporal circuit of macroscale dynamic brain activity supports human consciousness

Zirui Huang*, Jun Zhang*, Jinsong Wu, George A. Mashour, Anthony G. Hudetz

*Corresponding author. Email: huangzu@med.umich.edu (Z.H.); snapzhang@aliyun.com (J.Z.)

Published 11 March 2020, *Sci. Adv.* **6**, eaaz0087 (2020)
DOI: 10.1126/sciadv.aaz0087

The PDF file includes:

Fig. S1. *k*-means clustering approach and evaluations of *k*.
Fig. S2. CAPs identified from $k = 2$ to $k = 16$ with and without GSR.
Fig. S3. Spatial characteristics of the CAPs.
Fig. S4. Scatterplots and statistics for the Spearman rank correlations between the occurrence rate of joint mirror motifs or individual CAPs and the level of responsiveness.
Fig. S5. CAP occurrence rates of different conditions from $k = 4$ to $k = 12$ with and without GSR.
Fig. S6. In-degree CAP accessibility of different conditions from $k = 4$ to $k = 12$ with and without GSR.
Fig. S7. Classifying conscious versus unresponsive states using SVM.
Fig. S8. Conventional static functional connectivity.
Fig. S9. The association between CAP occurrence rates and anticorrelations from $k = 4$ to $k = 12$ with and without GSR.
Table S1. A summary of statistics for Fig. 2 (B to E).

Other Supplementary Material for this manuscript includes the following:

(available at advances.sciencemag.org/cgi/content/full/6/11/eaaz0087/DC1)

Movie S1 (mp4 format). CAP temporal dynamics.

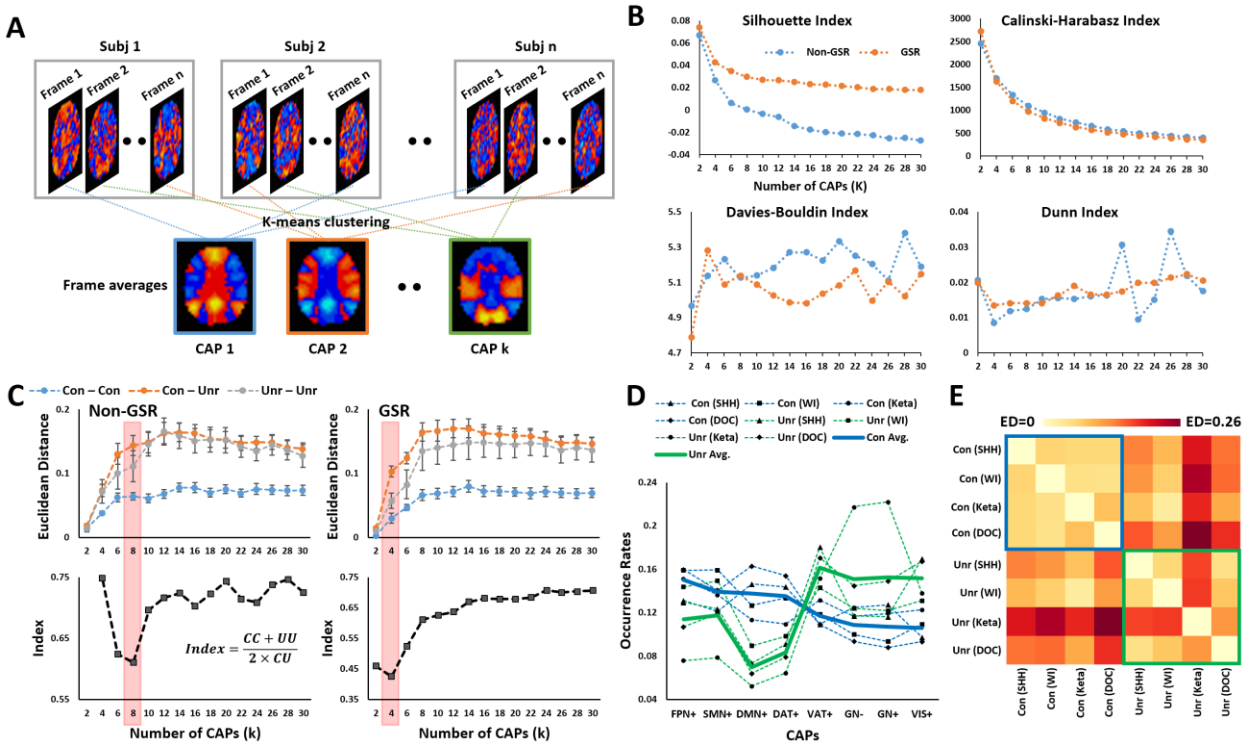

Fig. S1. *k*-means clustering approach and evaluations of *k*. (A) An illustration of k-means clustering algorithm that partitions the image volumes into k co-activation patterns (CAPs) across the entire dataset. **(B)** Evaluating the clustering performance using Silhouette, Calinski-Harabasz, Davies-Bouldin, and Dunn indices for the data without (non-GSR) and with GSR. Broadly speaking, higher values of the Silhouette, Calinski-Harabasz and Dunn, and a lower value of the Davies-Bouldin will indicate a better separation of clusters and more tightness inside the clusters. Collectively, different clustering evaluation criteria yielded inconsistent recommendations, in line with a previous study by Liu et al. *(22)*. **(C)** An optimized k (from a search between 2 and 30) was determined by trading off the inter-dataset similarity (measured by Euclidean distance) of the averaged CAP occurrence rate distributions in each dataset. Accordingly, an index, (CC+UU)/(2xCU), was defined as the ratio of inter-dataset similarity among conscious conditions (CC) and among unresponsive conditions (UU) versus the inter-dataset similarity among conscious and unresponsive conditions (CU) across the four datasets. Eight CAPs (for non-GSR) and four CAPs (for GSR) yielded a high inter-dataset similarity between conscious conditions and between unresponsive conditions, with a low inter-dataset similarity between conscious and unresponsive conditions. **(D)** The occurrence rate distributions across eight CAPs (k=8, non-GSR) for conscious (Con) and unresponsive (Unr) conditions in Dataset 1 (SHH), Dataset 2 (WI), Dataset 3 (Keta), Dataset 4 (DOC; neuropathological patients), and their averaged distributions (Avg.) across four datasets. **(E)** The Euclidian distance (ED) of the occurrence rate distributions between conditions.

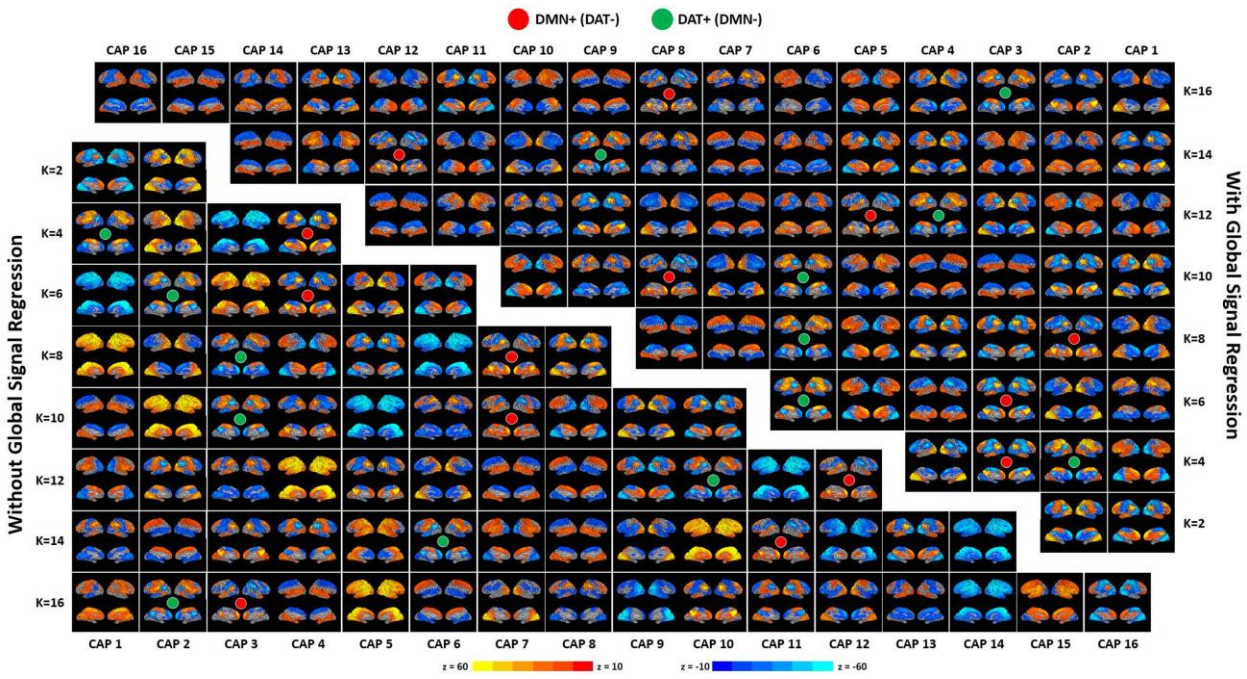

Fig. S2. CAPs identified from *k* = 2 to *k* = 16 with and without GSR. The choice of k=8 leads to the maximal number of identifiable networks, which are conserved when k>8. The DMN+ and DAN+ were defined from K=8, no-GSR (as main results shown in Fig. 1). Using the centroids of the two CAPs, we identified comparable DMN+ and DAN+ patterns in other CAP sets based on maximal similarity of the corresponding centroids.

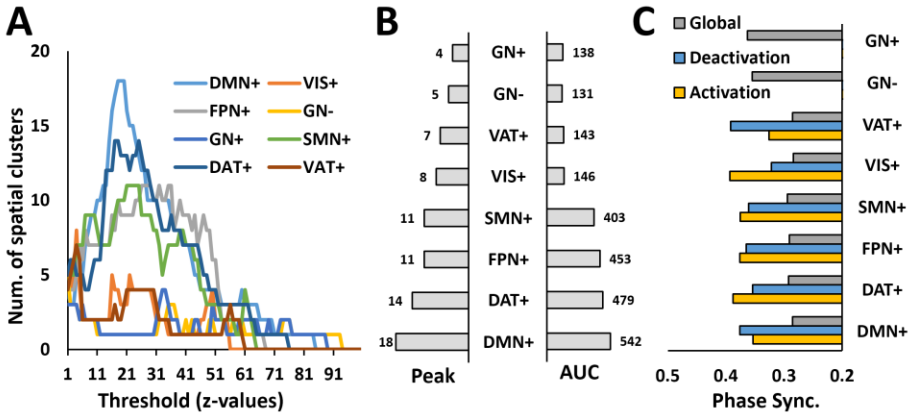

Fig. S3. Spatial characteristics of the CAPs. (A) The number of spatial clusters changes as a function of threshold (z-values) for all the CAPs (k=8, non-GSR). **(B)** The peak and area under the curve (AUC) of the number of spatial clusters. **(C)** The instantaneous phase synchronization values (Phase Sync.) for all CAPs and their corresponding activated and deactivated regions within each CAP. The GN+ and GN- show the highest global phase synchronization among all CAPs. Although the global phase synchronization is relatively low for DMN+ and DAT+, their intra-cluster phase synchronizations are as high as those of GN+ and GN-.

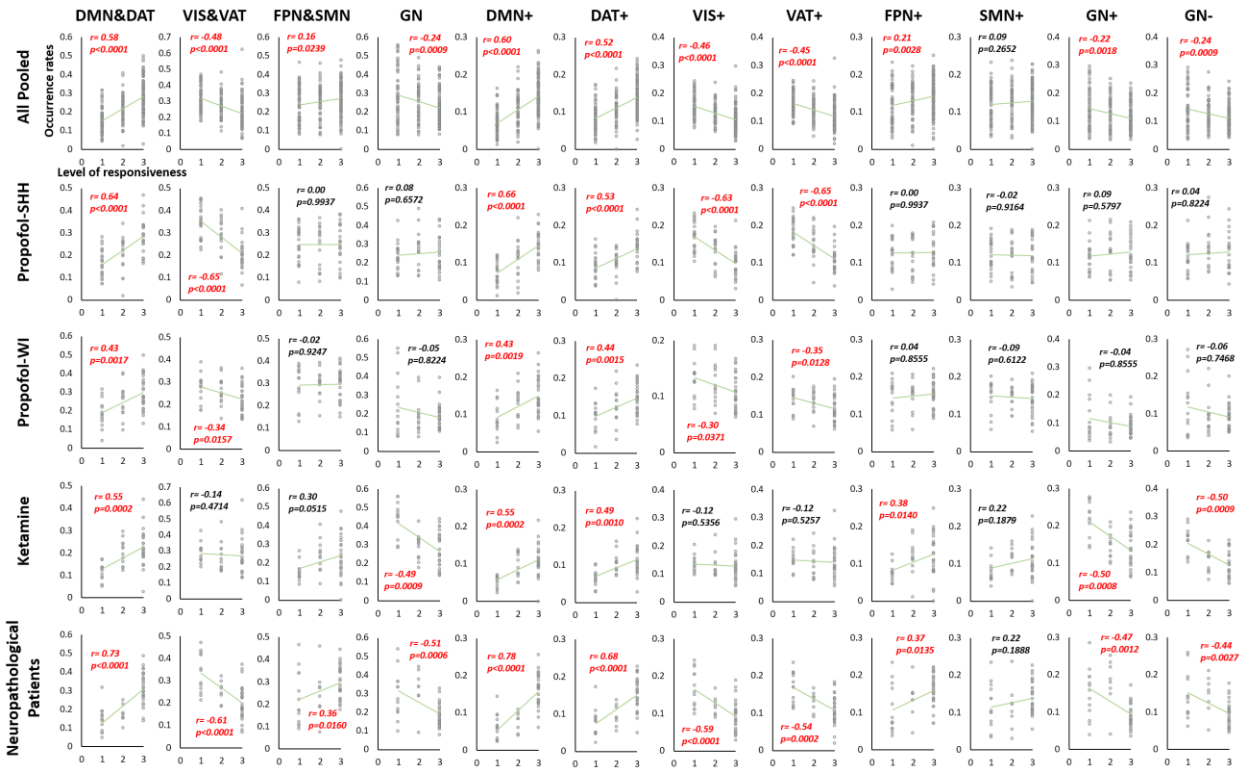

Fig. S4. Scatterplots and statistics for the Spearman rank correlations between the occurrence rate of joint mirror motifs or individual CAPs and the level of responsiveness. Conscious and recovery conditions were ranked at 3, intermediate conditions (propofol light sedation, PreLOR of ketamine induction and MCS patients) were ranked at 2, and unresponsive conditions (propofol general anesthesia and deep sedation, LOR due to ketamine, and UWS patients) were ranked as 1. P values are FDR-corrected at $\alpha < 0.05$.

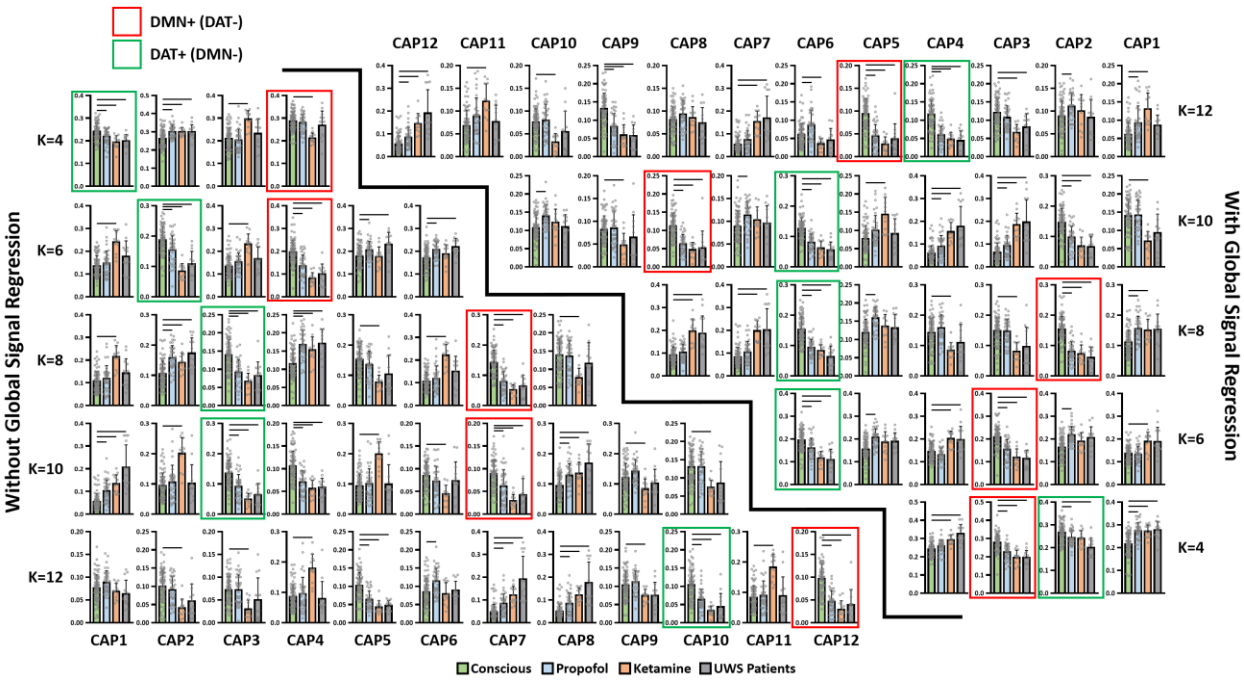

Fig. S5. CAP occurrence rates of different conditions from *k* = 4 to *k* = 12 with and without GSR. We collapsed the conscious conditions across the four datasets, and collapsed propofol-induced unresponsiveness of propofol-SHH and propofol-WI, to reduce the complexity of comparisons. As a result, we had four conditions with one conscious and three unresponsive conditions: propofol, ketamine, and patients with UWS. Comparisons of the CAP occurrence rates for conscious vs. propofol, conscious vs. ketamine, and conscious vs. patients with UWS were performed by two-sided Student t-tests. Black lines on top of the bars indicate significance at FDR-corrected $\alpha < 0.05$. Note that the reduction of occurrence rates of DMN+ and DAN+ during unresponsiveness is robust to the selection of k and the choice of non-GSR or GSR.

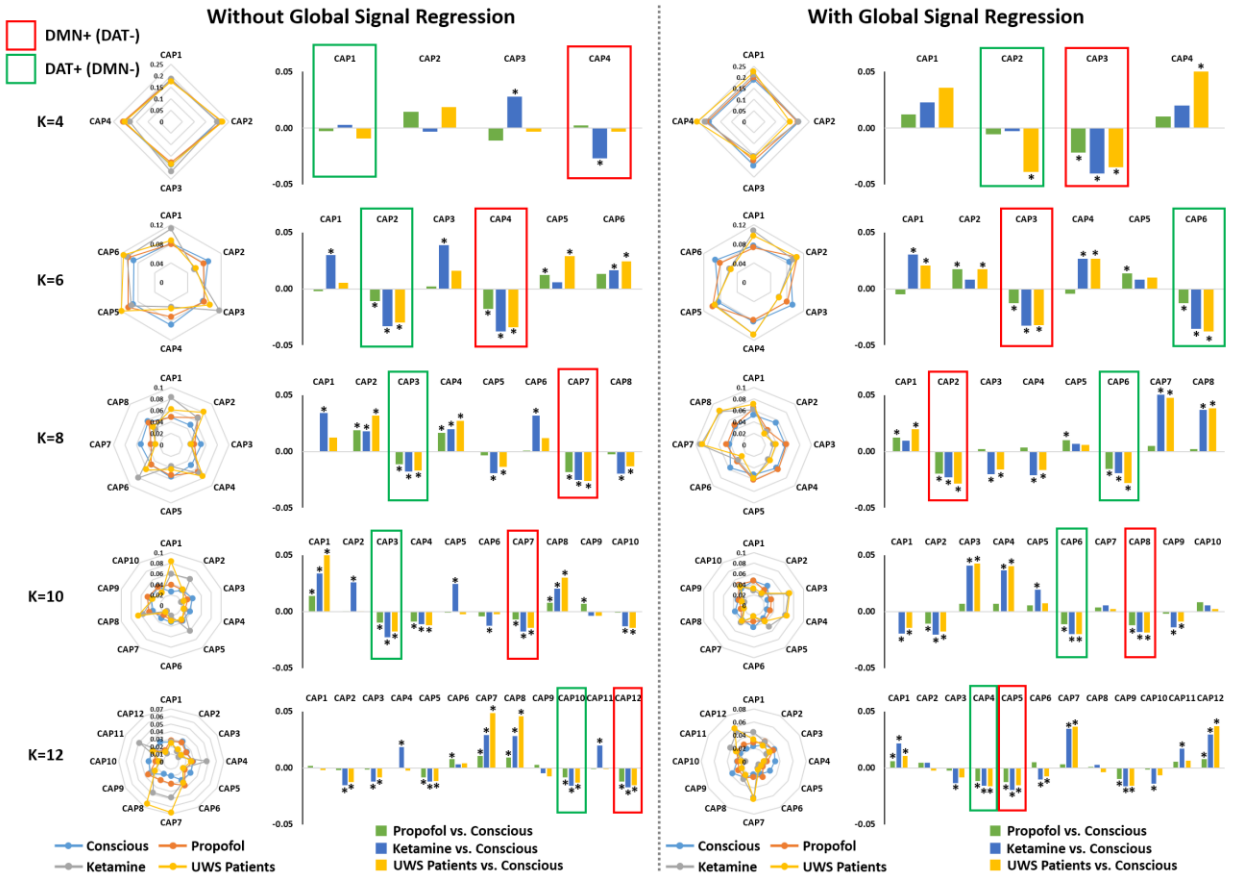

Fig. S6. In-degree CAP accessibility of different conditions from *k* = 4 to *k* = 12 with and without GSR. Descriptive complexity of trajectories (in bits) was first calculated between each pair of CAPs in conscious condition (conscious), propofol-induced unresponsiveness (propofol), ketamine-induced unresponsiveness (ketamine), and in patients with unresponsive wakefulness syndrome (UWS). The accessibility of each CAP was defined as the inverse of descriptive complexity. The in-degree accessibility of each CAP (final CAP) was then calculated by averaging its accessibility from each starting point (initial CAPs); as an example, the node size in Fig. 4. Radar plots show the in-degree CAP accessibility for different conditions. Bar plots show the differences of in-degree CAP accessibility for propofol vs. conscious, ketamine vs. conscious, and patients with UWS vs. conscious. Non-parametric permutation tests were used to assay the differences between conditions. The null models were generated by 1000 permutations across the entire dataset (see more details in Materials and Methods). Significance level was determined at $p<0.001$ by considering multiple comparison corrections (99.9th and 0.1th percentile of the null distributions, two-sided). Note that both DMN+ and DAN+ showed a consistent decrease of in-degree accessibility during unresponsiveness, which was robust with respect to the choice of k and to the option of non-GSR or GSR.

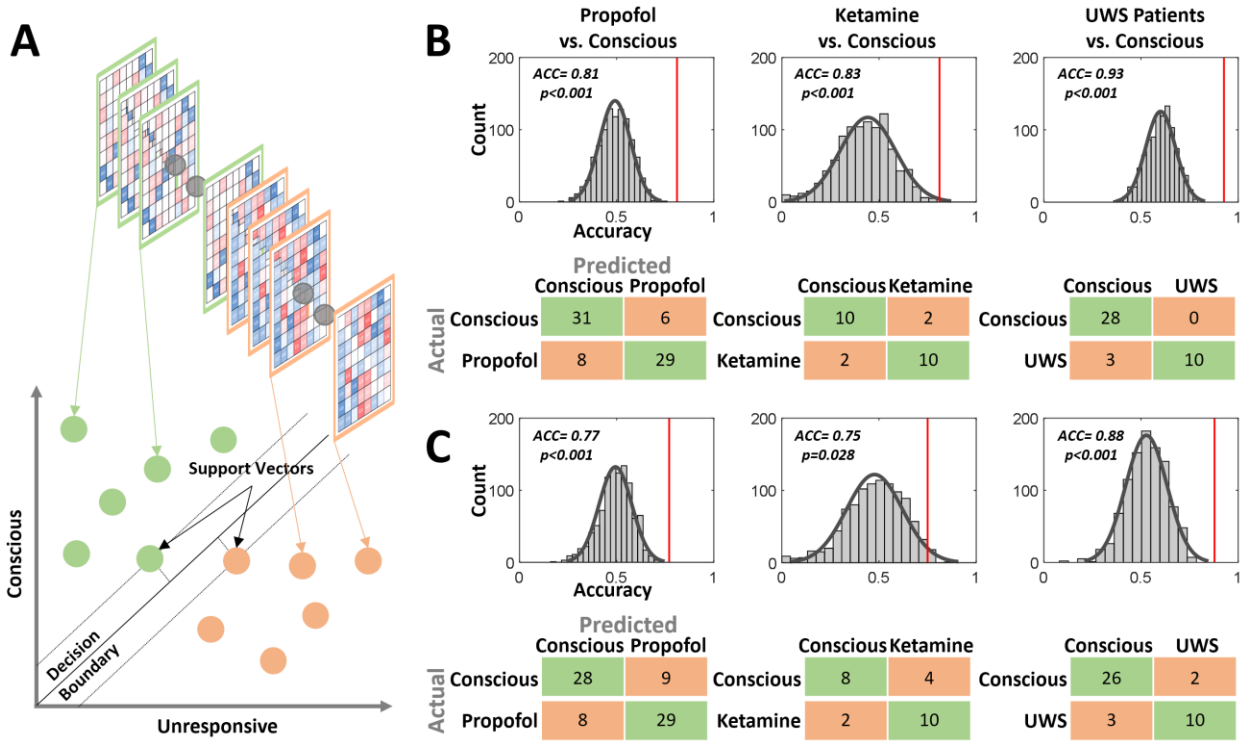

Fig. S7. Classifying conscious versus unresponsive states using SVM. (A) Schematic representation of the support vector machine (SVM). SVM is a discriminative model that generates a hyperplane (i.e., decision boundary) that maximizes the separation between two classes in an N-dimensional space of features. The hyperplane is defined by support vectors. The features are based on the transition probability **(B)** and entropy of Markov trajectory **(C)** matrices estimated from individual subjects. These matrices were used to train and test the SVM classifier via leave-one-subject-out cross-validation procedure. Statistical significance of the classification accuracy was tested by permutations, i.e., shuffling the class labels 1000 times for a given contrast. Confusion matrices (actual vs. predicted) are shown.

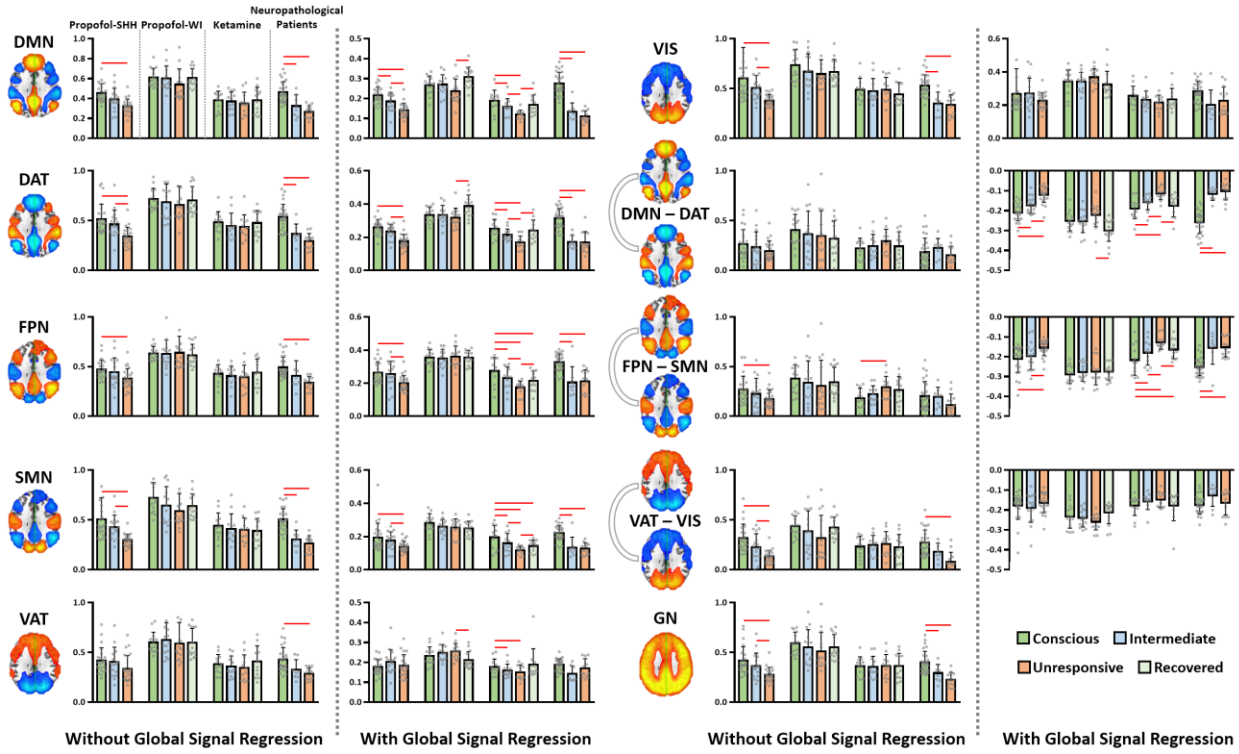

Fig. S8. Conventional static functional connectivity. According to the main CAP results (k=8, no-GSR), we defined seven networks including DMN, DAT, FPN, SMN, VAT, VIS and GN, by extracting the positive voxels (neglecting deactivations) within each CAP. Within-network and between-network (for mirror motifs) functional connectivity was calculated and presented with and without global signal regression (GSR). Intermediate conditions refer to propofol light sedation, PreLOR of ketamine induction and patients with MCS, and unresponsive conditions refer to propofol general anesthesia and deep sedation, LOR due to ketamine, and patients with UWS. Red lines indicate significance at FDR-corrected $\alpha < 0.05$. Note that the anticorrelation relationship between networks was only seen when GSR was applied. Error bars indicate ±SD.

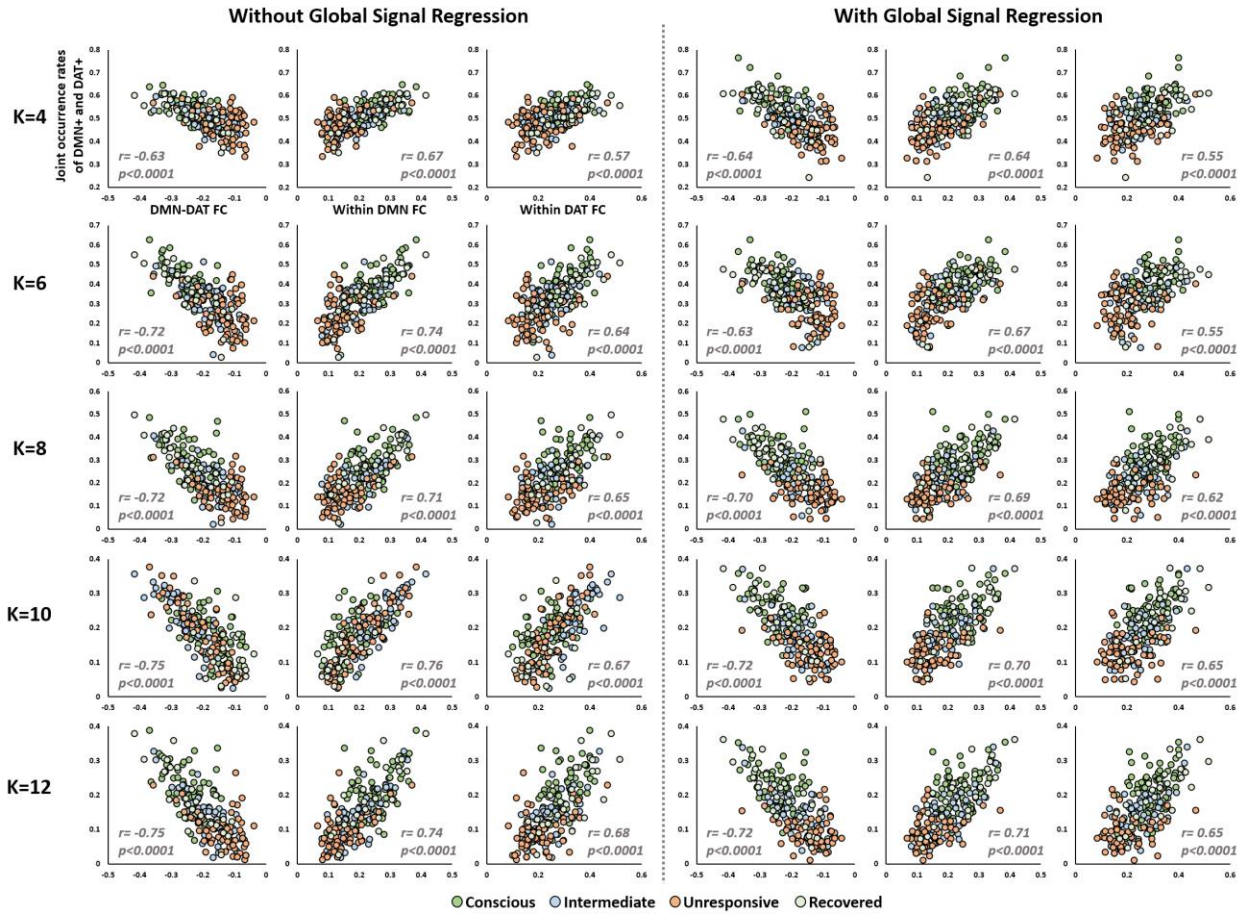

Fig. S9. The association between CAP occurrence rates and anticorrelations from *k* = 4 to *k* = 12 with and without GSR. We calculated Pearson correlations between the joint occurrence rates of DMN+ and DAT+ (both non-GSR and GSR) and the strength of DMN-DAT functional connectivity (after GSR), as well as within-network functional connectivity (after GSR) of DMN and DAT across all subjects. Intermediate conditions refer to propofol light sedation, PreLOR of ketamine induction and patients with MCS, and unresponsive conditions refer to propofol general anesthesia and deep sedation, LOR due to ketamine, and patients with UWS.

Table S1. A summary of statistics for Fig. 2 (B to E).

FDR corrected p values		DMN+	DAT+	VIS+	VAT+	FPN+	SMN+	GN+	GN-
Propofol-SHH	C vs. LS	0.120	0.035	0.061	0.061	0.382	0.404	0.318	0.742
	C vs. GA	0.000	0.001	0.000	0.000	0.918	0.865	0.654	0.483
	LS vs. GA	0.152	0.747	0.263	0.382	0.489	0.448	0.382	0.621
Propofol-WI	C vs. LS	0.828	0.643	0.364	0.263	0.560	0.249	0.767	0.850
	C vs. DS	0.036	0.152	0.237	0.193	0.308	0.339	0.382	0.293
	C vs. ROR	0.047	0.170	0.747	0.689	0.382	0.734	0.290	0.828
	LS vs. DS	0.020	0.179	0.807	0.747	0.515	0.800	0.289	0.260
	LS vs. ROR	0.071	0.119	0.179	0.152	0.952	0.247	0.574	0.982
	DS vs. ROR	0.000	0.004	0.038	0.023	0.698	0.055	0.152	0.179
Ketamine	C vs. PreLOR	0.152	0.699	0.773	0.489	0.035	0.193	0.061	0.047
	C vs. LOR	0.002	0.014	0.289	0.263	0.005	0.020	0.001	0.001
	C vs. ROR	0.539	0.699	0.379	0.364	0.032	0.021	0.112	0.004
	PreLOR vs. LOR	0.017	0.008	0.260	0.455	0.035	0.035	0.004	0.002
	PreLOR vs. ROR	0.747	0.575	0.620	0.643	0.237	0.039	0.620	0.467
	LOR vs. ROR	0.035	0.032	0.966	0.982	0.283	0.782	0.011	0.018
DOC	HC vs. MCS	0.000	0.004	0.087	0.198	0.382	0.406	0.048	0.027
	HC vs. UWS	0.000	0.000	0.002	0.002	0.049	0.382	0.047	0.034
	MCS vs. UWS	0.448	0.382	0.044	0.049	0.382	0.879	0.953	0.472

Note: Paired t-tests for propofol-SHH, propofol-WI and ketamine and unpaired t-tests for neuropathological patients (disorders of consciousness; DOC) were performed. C: baseline conscious condition; LS: light sedation; GA: general anesthesia; DS: deep sedation; ROR: recovery of responsiveness; PreLOR: pre-loss-of-responsiveness; LOR: loss of responsiveness; HC: healthy control; MCS: minimally consciousness state; UWS: unresponsive wakefulness syndrome. Red font highlights significant results at FDR-corrected $\alpha < 0.05$.